

Quantum Elliptic Vortex in a Nematic-Spin Bose-Einstein Condensate

Hiromitsu Takeuchi*

*Department of Physics and Nambu Yoichiro Institute of Theoretical and Experimental Physics (NITEP),
Osaka City University, Osaka 558-8585, Japan*

(Dated: May 14, 2021)

We find a novel topological defect in a spin-nematic superfluid theoretically. A quantized vortex spontaneously breaks its axisymmetry, leading to an elliptic vortex in nematic-spin Bose-Einstein condensates with small positive quadratic Zeeman effect. The new vortex is considered the Joukowski transform of a conventional vortex. Its oblateness grows when the Zeeman length exceeds the spin healing length. This structure is sustained by balancing the hydrodynamic potential and the elasticity of a soliton connecting two spin spots, which are observable by *in situ* magnetization imaging. The theoretical analysis clearly defines the difference between half quantum vortices of the polar and antiferromagnetic phases in spin-1 condensates.

Topological defects (TDs) caused by spontaneous symmetry breaking (SSB) phase transition is ubiquitous, existing as skyrmions in spintronic devices [1], vortices in superconductors and superfluids [2, 3], and even disclinations in LCD displays [4]. Thanks to the universal concept of SSB, TDs in laboratories are useful for simulating TDs in other exotic settings, the early universe, the dense matters in compact stars, and higher-dimensional spacetimes in field theory [5–8]. Multicomponent superfluids with spin freedom, such as spin-triplet superfluid ^3He and binary and spinor Bose-Einstein condensates (BECs) [9–12], are powerful tools to develop theories of TDs since various TDs are realized there. Such superfluids are called the nematic-spin superfluids [13], whose order state is partly represented by a vector $\hat{\mathbf{d}}$ that mimics the *director* $\hat{\mathbf{d}}$ in nematic liquid crystals (NLCs) [4].

Nematic-spin superfluids support not only conventional TDs in NLCs (disclination, hedgehog, domain wall, and boojum [14–24]), but also novel TDs combined with the superfluidity, e.g., half quantum vortex (HQV) [25]. The term HQV is used also in exciton-polariton condensates [26, 27]. The simplest type of HQV has been realized experimentally in different superfluids [28–30], where the core of a vortex in a spin component is occupied by other components. A nontrivial HQV is terminated by a domain wall across which the order-parameter phase jumps by π . The wall-HQV composites were first realized as the double-core vortices in $^3\text{He-B}$ [31] and revisited [32–34], motivated by the early Universe scenario nucleating the composites of the Kibble-Lazarides-Shafi (KLS) walls and cosmic strings [35–37]. Recently, the nonequilibrium dynamics of wall-HQV composites were observed in phase transition from the antiferromagnetic (AF) phase to the polar (P) phase [38] in a spin-1 ^{23}Na BEC [39, 40]. However, the dynamics are poorly understood, because of the lack knowledge about properties of wall-HQV composites. Determining these properties is important for understanding KLS-wall-HQV composites and double-core vortices in $^3\text{He-B}$ [41–45], the Berezinskii-Kosterlitz-Thouless transition in spinor BECs [46–48], and even the quark-confinement

problem in hadronic physics connected with the vortex-confinement problem [49–52].

Here, it is theoretically shown that a wall-HQV composite in spin-1 BECs [39, 40] takes an exotic state in equilibrium with a small positive quadratic Zeeman effect. This state, called the elliptic vortex, is hydrodynamically considered the Joukowski transform of a conventional vortex and has an elliptic structure with spin spots (Fig. 1). The spots are confined to the elliptic-vortex core and stabilized by a balance between the hydrodynamic effect and the tension of a domain wall or a soliton spanned between the spots.

Formulation.—A spin-1 BEC is described by the condensate wave function Φ_m ($m = 0, \pm 1$) of the $|m\rangle$ Zeeman component in the Gross-Pitaevskii model [12, 53]. The thermodynamic energy is represented as $G(\{\Phi_m\}) = \int d^3x \mathcal{G}$, with $\mathcal{G} = \frac{\hbar^2}{2M} \sum_m |\nabla \Phi_m|^2 + \mathcal{U}$, and

$$\mathcal{U} = \frac{c_0}{2} n^2 + \frac{c_2}{2} \mathbf{s}^2 - (\mu - q)n - q|\Phi_0|^2 - p s_z. \quad (1)$$

Here, we introduced the chemical potential $\mu (> 0)$ and the coefficient q (p) of the quadratic (linear) Zeeman effect. In the Cartesian representation $\Phi = [\Phi_x, \Phi_y, \Phi_z]^T = \left[\frac{-1}{\sqrt{2}}(\Phi_{+1} - \Phi_{-1}), \frac{-i}{\sqrt{2}}(\Phi_{+1} + \Phi_{-1}), \Phi_0 \right]^T$ [54], the condensate density is expressed by the dot product $n = \sum_m |\Phi_m|^2 = \Phi^* \cdot \Phi$ and the spin density by the cross product $\mathbf{s} = [s_x, s_y, s_z]^T = i\Phi \times \Phi^*$.

The ground (bulk) state is obtained by minimizing $U = \int d^3x \mathcal{U}$. Assuming $c_2 = 0.016c_0 > 0$ with $p = 0$ obtained experimentally [39, 40], the ground state is in the P state $\Phi = \Phi_P = [0, 0, \sqrt{n_P} e^{i\theta_G}]^T$ with the bulk density $n_P = \frac{\mu}{c_0}$ and the order-parameter phase θ_G . By rescaling energy and length by μ and $\xi_n \equiv \frac{\hbar}{\sqrt{M\mu}}$, respectively, the P phase is parametrized by two dimensionless quantities $\frac{c_2}{c_0}$ and $\frac{q}{\mu}$.

Vortex core structure.—One might expect that there is nothing strange about the occurrence of vortices in P phase, whose order parameter (OP) is a complex scalar $\Phi_0 (= \Phi_z)$ with $\Phi_{\pm 1} = 0$, as in conventional superfluids. However, the core of a singly quantized vortex can be

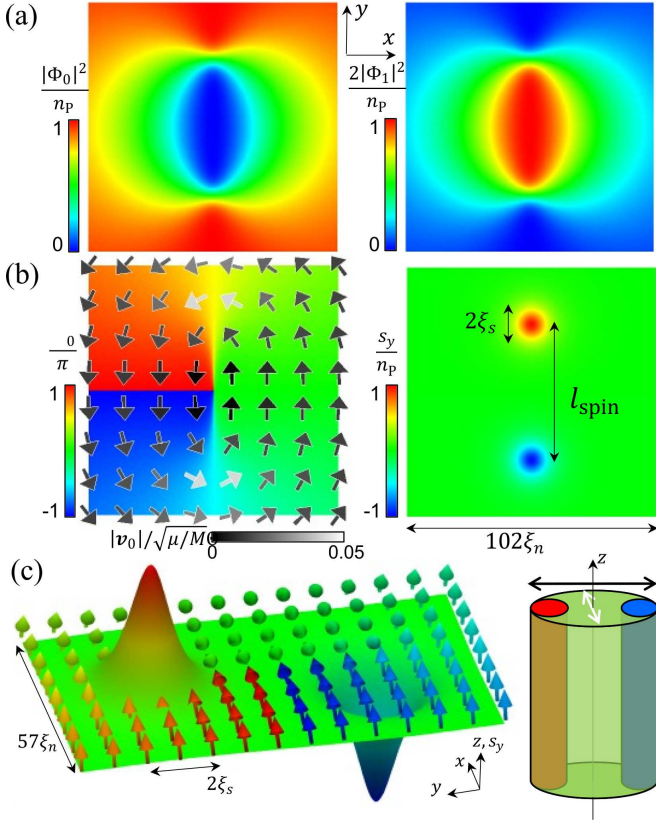


FIG. 1. The cross-sectional profile of an elliptic vortex for $q/\mu = 2^{-17} \approx 7.6 \times 10^{-6}$. (a) The left and right sides show the profiles of $\frac{|\Phi_0|^2}{n_p}$ and $\frac{|\Phi_1|^2}{2n_p}$, respectively. The density $|\Phi_{-1}|^2$ (not shown) is the same as $|\Phi_1|^2$. (b) The vector field on the left shows $\mathbf{v}_0 = \frac{\hbar}{M} \nabla \Theta_0$, with the background plot of $\Theta_0 = \arg \Phi_0$. The phase $\arg \Phi_{\pm 1}$ is homogeneous inside the core (not shown). The spin density s_y is plotted on the right, while $s_x = s_z = 0$. (c) Left: the texture of the unit vector $\mathbf{g}/|\mathbf{g}|$ (arrow) in Eq. (3). The color of the arrows and the surface correspond to Θ_0 and s_y in (b), respectively. Right: schematic of the three-dimensional structure of the vortex core. The distance l_{spin} between the two spin spots with opposite transverse magnetization (blue and red) is determined by the balance between the hydrodynamic potential and the elastic potential by the AF soliton (green). The width ($\sim l_{\text{spin}}$) and thickness of the core are represented by black and white arrows, respectively.

unconventional in multicomponent superfluids, occupied by other components so as to reduce the condensation energy, e.g., $^3\text{He-B}$ at high pressure [55] and segregated binary BECs [56]. Similarly, the vortex core can be occupied by the $m = \pm 1$ component in the P phase.

To examine the conjecture, the lowest-energy solution was obtained by numerically minimizing G in the steepest descent method [57]. It is found that a nonaxisymmetric core structure is observed for small q/μ . Figure 2 shows the typical cross-sectional profile of the vortex for $\frac{q}{\mu} = 2^{-17}$ in a cylindrical flat-bottom potential of sufficiently large radius [58]. The vortex core is occupied by

the $m = \pm 1$ components, and the density n is mostly homogeneous [Fig. 1(a)]. Surprisingly, the velocity field forms an elliptic structure, and two spin spots are observed with opposite transverse magnetization ($s_y \neq 0$) at the edges of the core [Fig. 1(b)]. Since the order-parameter phase $\Theta_0 (= \arg \Phi_0)$ jumps by π across the $x = 0$ plane and rotates by π around each spin spot, this structure is regarded as a wall-HQV composite composed of a wall and two HQVs with the same circulation.

The distance l_{spin} between the spin spots is a decreasing function of q [Fig. 2(a)]. Accordingly, the density n_{core} at the center of the vortex core and the maximum spin density s_{\perp}^{max} decrease with q and vanish at a critical value $q_C \approx 0.25\mu$ [Fig. 2(b)] [59, 60]. This behavior is similar to that of the AF-core soliton [61], where the soliton core is vacant for large q but occupied by the local AF state ($\mathbf{s} = 0$ with $\Phi_{\pm 1} \neq 0$ and $\Phi_0 \approx 0$) for small q . In our case, however, the vortex core is occupied by two different states, the local broken-axisymmetry (BA) state ($\mathbf{s} \perp \hat{z}$ with $\Phi_1 \Phi_0 \Phi_{-1} \neq 0$) and the local AF state.

In order to explain the nematic-spin order in the vortex core, we extend the OP space as

$$\Phi = \sqrt{n} e^{i\theta_G} \hat{\mathbf{d}}, \quad (2)$$

which represents the OP in the ground state with $\mathbf{s} = 0$ for $q = 0$. The real unit vector $\hat{\mathbf{d}}$ is called the *pseudodirector*; the state of $(\hat{\mathbf{d}}, \theta_G)$ is identical to $(-\hat{\mathbf{d}}, \theta_G + \pi)$. In terms of the extended OP, the ground state in the P (AF) phase with $q > 0$ ($q < 0$) is represented as $n = n_p$ and $\hat{\mathbf{d}} = \pm \hat{z}$ ($n = n_{\text{AF}}$ and $\hat{\mathbf{d}} = \hat{\mathbf{r}}_{\perp}$) within the unit vector \hat{z} ($\hat{\mathbf{r}}_{\perp}$) parallel (normal) to the quantization axis and the density $n_{\text{AF}} = \frac{\mu - q}{c_0}$ of the AF state. To describe the magnetization together with the nematic-spin order, it is useful to introduce a representation

$$\Phi = e^{i\Theta_0} (\mathbf{g} + i\mathbf{h}) \quad (3)$$

with $\mathbf{g} = [g_x, g_y, g_z]^T$ with $g_z \geq 0$ and $\mathbf{h} \perp \hat{z}$. Equation (3) reduces Eq. (2) for $\mathbf{s} = 2\mathbf{g} \times \mathbf{h} = 0$ with $\mathbf{g} = \sqrt{n} \hat{\mathbf{d}}$. The left panel in Fig. 1(c) shows a cross-sectional plot of $\frac{\mathbf{g}}{|\mathbf{g}|}$ and s_y . In the region between the spin spots, \mathbf{g} lies on the xy plane forming the local AF state, where the state $(\hat{\mathbf{d}}, \Theta_0) = (-\hat{\mathbf{x}}, \pm\pi)$ for $x > 0$ is identical to $(\hat{\mathbf{x}}, 0)$ for $x < 0$ along the yz plane. The nematic-spin order is destroyed when $\hat{\mathbf{d}}$ is ill-defined in the spin spots occupied by the local BA state [see the right panel in Fig. 1(c)].

To clarify our problem, the main goal is to answer the following two questions:

Q1: What causes the axisymmetry breaking?

Q2: What is the physical mechanism to stabilize the elliptic structure?

Vortex winding rule.—As the answer for the first question, it is claimed that the spin interaction breaks the axisymmetry. To justify the claim logically, we introduce a winding rule of an axisymmetric vortex in spin-1

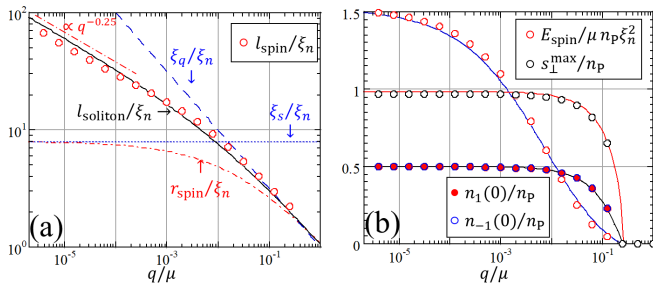


FIG. 2. (a) The q dependence of l_{spin} . The solid curve represents the evaluation by Eq. (12). All lengths are rescaled by ξ_n . (b) The q dependence of the spin interaction E_{spin} , the maximum spin density $s_{\perp}^{\text{max}} = \max(s_y)$, and the core density $n_{\pm 1}(0)$. The solid curve tracing the data corresponds to an analytic formula (see text).

BECs. We consider a straight vortex along the z axis, the cross section of which is axisymmetric as the ansatz $\Phi_m = f_m(r)e^{iL_m\varphi}$, with radius $r = \sqrt{x^2 + y^2}$, and azimuthal angle φ in cylindrical coordinates. The rule states that L_m is parametrized by the winding numbers L and N , associated with the mass and spin current, respectively, and given by

$$L_m = L + mN \quad (L, N = 0, \pm 1, \pm 2, \dots). \quad (4)$$

The rule is related to the phase factor $\delta\Theta = (L_{+1} + L_{-1} - 2L_0)\varphi$. By substituting the ansatz into the equation of motion, we have, for the equation of Φ_0 , $0 = (h_0 - \mu + c_0n + c_2f_{+1}^2 + c_2f_{-1}^2 + 2c_2f_{+1}f_{-1}e^{i\delta\Theta})f_0$. The last term comes from the transverse spin density and the equation of real function f_m is solved when $e^{i\delta\Theta} = \pm 1$, resulting in Eq. (4). Therefore, this rule is applicable for $s_x \neq 0$ or $s_y \neq 0$ with $f_{+1}f_{-1}f_0 \neq 0$ [62].

By contraposition of the above argument, the vortex must be nonaxisymmetric, when the winding rule is not satisfied. As seen in Fig. 1, only the $m = 0$ component has a nonzero winding number, corresponding to $L_0 = 1$ and $L_{\pm 1} = 0$. Such a set of winding numbers cannot satisfy the winding rule. The axisymmetry is exactly recovered only for $\Phi_{\pm 1} = 0$ ($q \geq q_C$). Since the winding rule works for $s_x \neq 0$ or $s_y \neq 0$, the transverse magnetization appear as a manifestation of the axisymmetry breaking. The orientations of the transverse spin and the axes of the elliptic structure depend on the phases $\arg \Phi_m$.

Joukowski mapping.—To answer the second question, the potential flow theory in two-dimensional flow is extended to our problem. The elliptic core structure hints at the Joukowski transformation [63], since the velocity field on the cross section is considered a two-dimensional potential flow. This perception is the motivation for investigating the problem, and the following analysis leads to a quantitative evaluation of the core structure.

The velocity field $\mathbf{v}_0 = \frac{\hbar}{M}\nabla\Theta_0 = (u, v)$ in the xy plane is generated by a conformal mapping called the

Joukowski transformation from a vortex within a cylinder of radius a in the ζ complex plane to the xy plane, $x + iy = \zeta + \frac{a^2}{\zeta}$ [63]. By using the parametrization $\zeta = ia e^{\phi + i\psi}$ ($\phi \geq 0$), one obtains $(x, y) = 2a(\cosh\phi \cos(\psi + \pi), \sinh\phi \sin(\psi + \pi))$, representing an ellipse of width $4a \cosh\phi$ and thickness $4a \sinh\phi$.

The velocity field is computed by applying the conformal mapping to the complex velocity potential W of the vortex in the ζ plane,

$$W = -i\frac{\kappa}{2\pi} \log \zeta. \quad (5)$$

The circulation $\kappa = \frac{2\pi\hbar}{M}$ around a quantized vortex is conserved in the transformation as follows. By applying the transformation to Eq. (5) and using the formula $v \rightarrow \pm \frac{\kappa}{2\pi} \frac{1}{\sqrt{4a^2 - y^2}}$ for $|y| < 2a$ in the limit $x \rightarrow \pm 0$, the vorticity $\omega_z(x, y) = (\nabla \times \mathbf{v}_0)_z$ forms a segment singularity of width $4a$,

$$\omega_z(\mathbf{r}) = \frac{\kappa}{\pi} \frac{1}{\sqrt{4a^2 - y^2}} \delta(x) \Theta(2a - |y|). \quad (6)$$

with the step function Θ ($\Theta = 1$ for $2a \geq |y|$ and $\Theta = 0$ for $2a < |y|$). By integrating Eq. (6), it is confirmed that the circulation is conserved as $\int dx dy \omega_z = \kappa$.

Hydrodynamic potential.—To reveal the physical mechanism that stabilizes the elliptic vortex, the energy E_{vortex} of a vortex of unit length is evaluated. The vortex energy in the ζ plane is computed conventionally by considering the contribution from the core region ($|\zeta| < \rho_{\text{core}} \equiv ae^{\phi_{\text{core}}}$) and the outer region ($|\zeta| > \rho_{\text{core}}$) separately [3]. Similarly, we consider the Joukowski mapping of the former and the latter, corresponding to an ellipse of area S_{core} and outer area S_{out} in the xy plane, respectively.

The core region is characterized by two parameters a and $r_{\text{core}} \equiv \rho_{\text{core}} - a$ as

$$S_{\text{core}} = \pi R_+ R_- = \pi \frac{(a + r_{\text{core}})^4 - a^4}{(a + r_{\text{core}})^2}, \quad (7)$$

with $R_{\pm} = \frac{(a + r_{\text{core}})^2 \pm a^2}{a + r_{\text{core}}}$. Here, $2R_{+(-)}$ is the width (thickness) of the ellipse. For high oblateness with $\frac{a}{r_{\text{core}}} \gg 1$, we have $R_+ \approx 2a$ and $R_- \approx 2r_{\text{core}}$. The axisymmetric limit $\frac{a}{r_{\text{core}}} \rightarrow 0$ results in $R_+ = R_- \rightarrow r_{\text{core}}$.

The vortex energy is defined as the excess energy in the presence of the vortex, with respect to the bulk energy $E_{\text{bulk}} = \mathcal{U}_P(S_{\text{in}} + S_{\text{out}})$ with energy density $\mathcal{U}_P = -\frac{1}{2}\mu n_P$ in the bulk P phase. The vortex energy is then represented formally by

$$E_{\text{vortex}} = E_{\text{out}} + E_{\text{core}} - E_{\text{bulk}} = U_{\text{core}} + U_{\text{out}} \quad (8)$$

with $E_{\text{core(out)}} = \int_{S_{\text{core(out)}}} dx dy \mathcal{G}$ and $U_{\text{core(out)}} = E_{\text{core(out)}} - \mathcal{U}_P S_{\text{core(out)}}$. The potential U_{out} of the outer region is evaluated by computing the integral in E_{out} analytically with an approximation $n \approx n_P \left(1 - \frac{M}{2\mu} \mathbf{v}_0^2\right)$,

where the quantum pressure is neglected. In the approximation up to the order of $\mathcal{O}\left(\frac{M}{2\mu}v_0^2\right)$, a straightforward computation yields

$$U_{\text{out}} \approx U_{\text{hyd}} = \frac{Mn_{\text{P}}\kappa^2}{4\pi} \ln \frac{R}{a + r_{\text{core}}}. \quad (9)$$

Here, we used the radius $R = ae^{\phi_{\text{out}}}$ of the system boundary by assuming $R \gg a$ [64].

Elastic core potential.—The core potential U_{core} is determined by introducing a phenomenological model, where a soliton is spanned between the spin spots. This model is justified by the fact that the phase gradient is mainly concentrated around the spin spots, consistent with the vorticity distribution (6) [see also Fig. 1(b)]; thus, the core structure between the spots is similar to that of the AF-core soliton [61]. Accordingly, we write

$$U_{\text{core}} = E_{\text{soliton}} + E_{\text{spin}} \quad (10)$$

where the soliton energy E_{soliton} is a function of the soliton length $l_{\text{soliton}} \sim l_{\text{spot}}$ and the spin interaction E_{spin} comes from the second term of Eq. (1).

The spin interaction is determined independently from the hydrodynamic argument, and thus U_{core} depends explicitly on l_{spot} through E_{soliton} . The size r_{spin} and the magnitude $s_{\perp}^{\text{max}} = \max(s_y)$ of the spin spot are asymptotic to $\xi_s = \frac{\hbar}{\sqrt{Mc_2n_{\text{P}}}}$ and n_{P} , respectively, for $\xi_q \gg \xi_s \gg \xi_n$. For $\xi_s \gg \xi_q \gtrsim \xi_n$, the core density grows as $n_{\pm 1}(0) \propto 1 - \frac{q}{q_c}$ in the continuous phase transition [65], and the size r_{spin} must be bounded below the vortex core size $\lesssim \xi_q$. Therefore, the size of a spin spot is simply parametrized as

$$r_{\text{spin}}^{-1} = \xi_s^{-1} + C_{\text{spin}}\xi_q^{-1} \quad (11)$$

with $C_{\text{spin}} \sim \mathcal{O}(1)$. In fact, the spin interaction, estimated by $E_{\text{spin}} = \frac{1}{2}c_2(s_y^{\text{max}})^2\pi r_{\text{spin}}^2$ agrees well with the numerical result with $C_{\text{spin}} = 0.8$ [Fig. 2 (b)] [66].

To simplify the analysis, we write as $l_{\text{soliton}} \equiv 4a + 4r_{\text{core}}$. The equilibrium length is then determined by $\frac{\partial}{\partial l_{\text{soliton}}} E_{\text{vortex}} = \frac{\partial}{\partial l_{\text{soliton}}} (U_{\text{hyd}} + E_{\text{soliton}}) = 0$. In the first approximation, the soliton energy E_{soliton} is expressed as $E_{\text{soliton}}^{\text{first}} = \alpha_{\text{AF}}l_{\text{soliton}}$ with the tension coefficient $\alpha_{\text{AF}} \sim \sqrt{q\mu}n_{\text{P}}\xi_n$ of the AF-core soliton [61]. This approximation fails for $\xi_q \gg \xi_s$. Actually, the thickness of the elliptic core is much smaller than the thickness $\sim \xi_q$ of the AF-core soliton forming a halo structure [Fig. 1 (a)], which increases the tension effectively. To take this effect into account, we introduce a phenomenological formula

$$\frac{E_{\text{soliton}}}{\mu n_{\text{P}}\xi_n^2} = \sqrt{\frac{q}{\mu}} \frac{l_{\text{soliton}}}{\xi_n} \left(1 + \frac{l_{\text{soliton}}}{r_{\text{spin}}}\right). \quad (12)$$

This formula yields $\frac{l_{\text{soliton}}}{\xi_n} = \frac{r_{\text{spin}}}{4\xi_n} \left(\sqrt{1 + 8\pi \frac{\xi_q}{r_{\text{spin}}}} - 1\right)$ and explains the scaling behavior $l_{\text{soliton}} \sim l_{\text{spin}} \propto q^{-0.25}$

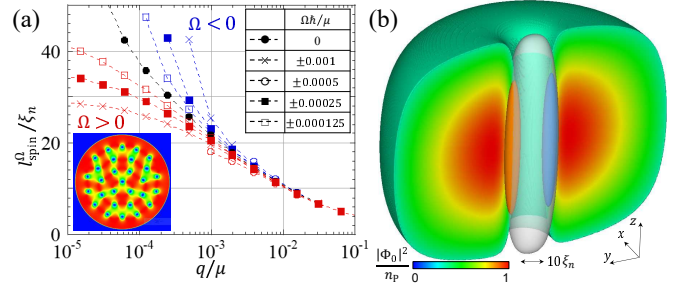


FIG. 3. (a) The q dependence of the width l_{spin}^{Ω} of a rotating elliptic vortex with angular velocity Ω . The single vortex is unstable for larger $|\Omega|$ and smaller q due the boundary effect. Inset: an elliptic-vortex lattice obtained after the instability due to the boundary effect for $\Omega\hbar/\mu = 0.001$ and $q/\mu = 2^{-11}$. (b) The three-dimensional solution of an elliptic vortex in a harmonic trap for $\Omega\hbar/\mu = 0.0005$. The isovolume plot shows the region $|\Psi_0|^2 c_0/\mu \leq 0.3$ for $x > 0$ with its $x = 0$ cross-sectional profile. A translucent surface along the z axis represents the isosurface of $|\Psi_{\pm 1}|^2 c_0/\mu = 0.15$, to which the two poles of the isosurfaces $s_y c_0/\mu = \pm 0.7$ are attached (red for positive and blue for negative).

for $\xi_q \gg \xi_s$ in Fig. 2(a). This means that the soliton is effectively elastic with $E_{\text{soliton}} \propto l_{\text{soliton}}^2$ for $l_{\text{spin}} \gg r_{\text{spin}}$.

Rotating solutions.—Finally, the response to an external rotation is investigated as a dynamical property. The external rotation of angular frequency Ω is described by the energy in the rotating frame $G' = G - \Omega L_z$, with the angular momentum L_z along the z axis [67]. The width l_{spin}^{Ω} of an elliptic vortex decreases with Ω [Fig. 3(a)], since the angular momentum increases more as the vorticity is localized more toward the center. Owing to the boundary effect [68], the single-vortex states are unstable for large $|\Omega|$ or small q/μ , leading to a lattice of elliptic vortices [inset of Fig. 3(a)].

The three-dimensional structure of an elliptic vortex is demonstrated numerically for a feasible setup in Fig. 3(b). A ^{23}Na BEC of 5.6×10^5 atoms is in a harmonic trap $V_{\text{trap}} = \frac{M}{2}(\omega_{\perp}^2 r^2 + \omega_z^2 z^2)$ with $\frac{\hbar}{\mu}(\omega_{\perp}, \omega_z) \approx (0.019, 0.024)$. The spin spots appear as two poles (red and blue) along the $m = \pm 1$ component (translucent pole) in the vortex core.

Discussion.—Although the wall-HQV composites were thought to be finally unstable, decaying into conventional axisymmetric vortices due to the snake instability of the wall [39, 40], the result suggests that they survive as elliptic vortices after the phase transition. The vortices including their dynamics will be observed through the transverse-spin spots by *in situ* magnetization imaging [29]. The theory here can be applied in a similar manner to the double-core vortex or the KLS-wall-HQV composite in $^3\text{He-B}$, while different forms of the hydrodynamic potential and soliton tension were introduced [69].

It is important to make a clear distinction between the types of HQVs in the AF phase (type I) and the P phase

(type II). Properties of type-I HQVs are understood by the following correspondence between binary BECs and the AF phase. Since the equation of motion of spin-1 BECs with $\Phi_0 = 0$ reduces to that of binary BECs, HQVs in miscible binary BECs are physically identical to type-I HQVs in the absence of the $m = 0$ component [29]; type-I HQVs with the same circulation are repulsive according to Ref. [70], where the intra- and inter-component coupling constants correspond to $g_1 = g_2 = c_0 + c_2$ and $g_{12} = c_0 - c_2$, respectively. Therefore, a pair of type-I HQVs are unstable without external rotation [71], which differs from type-II HQVs in that they form a bound pair by the wall tension [72–74].

It should be mentioned that similar composite objects are investigated experimentally as the spin-mass vortex attached by a planar soliton in $^3\text{He-B}$ [75, 76] and theoretically as the vortex molecules in Rabi-coupled binary BECs [49–52, 77–81]. Interestingly, the confinement of vortices by domain walls is considered a toy model of the quark-confinement problem [49]. Accordingly, “HQV-wall plasma”, an analog of quark-gluon plasma (QGP), occurs at a finite temperature T at least for $T > \frac{q}{k_B}$ in nematic-spin BECs, where thermal fluctuations free the spin spots from the confinement by the AF-core soliton. In this sense, the observed phase-transition dynamics [39, 40] are regarded as simulations of the transition dynamics from QGP to hadrons like the big bang simulation in ‘little bang’ [82]. Further investigations on the dynamics and interactions of elliptic vortices will shed light on unexplored phase-transition dynamics in different physical systems.

H.T. thanks Yong-il Shin for discussion and critical reading of the Letter. This work is supported by JSPS KAKENHI Grants No. JP17K05549, No. JP18KK0391, No. JP20H01842, and in part by the OCU “Think globally, act locally” Research Grant for Young Scientists through the hometown donation fund of Osaka City.

* takeuchi@osaka-cu.ac.jp; <http://hiromitsu-takeuchi.appspot.com>

- [1] Roland Wiesendanger. Nanoscale magnetic skyrmions in metallic films and multilayers: A new twist for spintronics, *Nat. Rev. Mater.* 1, 16044 (2016).
- [2] D. R. Tilley and J. Tilley. *Superfluidity and Superconductivity*. 2nd ed., Graduate Student Series in Physics (Adam Hilger, 1986).
- [3] Russell J Donnelly. *Quantized vortices in helium II*, volume 2. Cambridge University Press, 1991.
- [4] S. Chandrasekhar. *Liquid Crystals*. Cambridge University Press, 2 edition, 1992.
- [5] Alexander Vilenkin and E Paul S Shellard. *Cosmic strings and other topological defects*. Cambridge University Press, 2000.
- [6] Dany Page and Sanjay Reddy. Dense matter in compact stars: theoretical developments and observational constraints. *Annu. Rev. Nucl. Part. Sci.*, 56:327–374, 2006.
- [7] Tanmay Vachaspati. *Kinks and domain walls: An introduction to classical and quantum solitons*. Cambridge University Press, 2006.
- [8] ASHOKE SEN. Tachyon dynamics in open string theory. *International Journal of Modern Physics A*, 20(24):5513–5656, 2005.
- [9] Dieter Vollhardt and Peter Wolffe. *The superfluid phases of helium 3*. Courier Corporation, 2013.
- [10] Grigory E Volovik. *The universe in a helium droplet*, volume 117. Oxford University Press on Demand, 2003.
- [11] Kenichi Kasamatsu, Makoto Tsubota, and Masahito Ueda. Vortices in multicomponent Bose–Einstein condensates. *International Journal of Modern Physics B*, 19(11):1835–1904, 2005.
- [12] Yuki Kawaguchi and Masahito Ueda. Spinor Bose–Einstein Condensates. *Physics Reports*, 520(5):253–381, 2012.
- [13] The term “nematic-spin” or “spin-nematic” has been also used in the literature of different condensed matter systems, e.g., the spin-nematic phase in antiferromagnets [Hirokazu Tsunetsugu and Mitsuhiro Arikawa, *Spin Nematic Phase in S=1 Triangular Antiferromagnets*, *J. Phys. Soc. Jpn.* **75**, 083701 (2006)] and the nematic-spin fluid in BaFe_2As_2 [L. W. Harriger, H. Q. Luo, M. S. Liu, C. Frost, J. P. Hu, M. R. Norman, and Pengcheng Dai, *Nematic spin fluid in the tetragonal phase of BaFe2As2*, *Phys. Rev. B* **84**, 054544 (2011)]. .
- [14] N. D. Mermin. The topological theory of defects in ordered media. *Rev. Mod. Phys.*, 51:591–648, Jul 1979.
- [15] PB Sunil Kumar and GS Ranganath. On certain liquid crystal defects in a magnetic field. *Molecular Crystals and Liquid Crystals*, 177(1):131–144, 1989.
- [16] Grigory E Volovik. *Exotic properties of superfluid ^3He* , volume 1. World Scientific, 1992.
- [17] V. P. Mineyev and G. E. Volovik. Planar and linear solitons in superfluid ^3He . *Phys. Rev. B*, 18:3197–3203, Oct 1978.
- [18] Fei Zhou. Spin Correlation and Discrete Symmetry in Spinor Bose-Einstein Condensates. *Phys. Rev. Lett.*, 87:080401, Aug 2001.
- [19] Fei Zhou. Quantum spin nematic states in Bose–Einstein condensates. *International Journal of Modern Physics B*, 17(14):2643–2698, 2003.
- [20] J. Ruostekoski and J. R. Anglin. Monopole Core Instability and Alice Rings in Spinor Bose-Einstein Condensates. *Phys. Rev. Lett.*, 91:190402, Nov 2003.
- [21] N. D. Mermin. *Surface Singularities and Superflow in $^3\text{He-A}$* , pages 3–22. Springer US, Boston, MA, 1977.
- [22] GE Volovik. Defects at interface between A and B phases of superfluid ^3He . *JETP Lett*, 51(8):449, 1990.
- [23] T Sh Misirpashaev. The topological classification of defects at a phase interface. *Soviet physics, JETP*, 72(6):973–982, 1991.
- [24] Hiromitsu Takeuchi and Makoto Tsubota. Boojums in rotating two-component Bose-Einstein condensates. *Journal of the Physical Society of Japan*, 75(6):063601, 2006.
- [25] U. Leonhardt and G.E. Volovik. How to create Alice string (half quantum vortex) in a vector Bose-Einstein condensate. *Pisma Zh. Eksp. Teor. Fiz.*, 72:66–70, 2000.
- [26] Yuri G. Rubo. Half Vortices in Exciton Polariton Condensates. *Phys. Rev. Lett.*, 99:106401, Sep 2007.
- [27] K. G. Lagoudakis, T. Ostatnický, A. V. Kavokin, Y. G. Rubo, R. André, and B. Deveaud-Plédran. Observation

- of Half-Quantum Vortices in an Exciton-Polariton Condensate. *Science*, 326(5955):974–976, 2009.
- [28] M. R. Matthews, B. P. Anderson, P. C. Haljan, D. S. Hall, C. E. Wieman, and E. A. Cornell. Vortices in a Bose-Einstein Condensate. *Phys. Rev. Lett.*, 83:2498–2501, Sep 1999.
- [29] Sang Won Seo, Seji Kang, Woo Jin Kwon, and Yong-il Shin. Half-Quantum Vortices in an Antiferromagnetic Spinor Bose-Einstein Condensate. *Phys. Rev. Lett.*, 115:015301, Jul 2015.
- [30] S. Autti, V. V. Dmitriev, J. T. Mäkinen, A. A. Soldatov, G. E. Volovik, A. N. Yudin, V. V. Zavjalov, and V. B. Eltsov. Observation of Half-Quantum Vortices in Topological Superfluid ^3He . *Phys. Rev. Lett.*, 117:255301, Dec 2016.
- [31] Y. Kondo, J. S. Korhonen, M. Krusius, V. V. Dmitriev, Y. M. Mukharsky, E. B. Sonin, and G. E. Volovik. Direct observation of the nonaxisymmetric vortex in superfluid $^3\text{He-B}$. *Phys. Rev. Lett.*, 67:81–84, Jul 1991.
- [32] JT Mäkinen, VV Dmitriev, Jaakko Nissinen, Juho Rysti, GE Volovik, AN Yudin, Kuang Zhang, and VB Eltsov. Half-quantum vortices and walls bounded by strings in the polar-distorted phases of topological superfluid ^3He . *Nature communications*, 10(1):237, 2019.
- [33] G. E. Volovik and K. Zhang. String monopoles, string walls, vortex skyrmions, and nexus objects in the polar distorted B phase of ^3He . *Phys. Rev. Research*, 2:023263, Jun 2020.
- [34] K. Zhang. One-dimensional nexus objects, network of kibble-lazarides-shafi string walls, and their spin dynamic response in polar-distorted b -phase of ^3He . *Phys. Rev. Research*, 2:043356, Dec 2020.
- [35] T. W. B. Kibble, G. Lazarides, and Q. Shafi. Walls bounded by strings. *Phys. Rev. D*, 26:435–439, Jul 1982.
- [36] T.W.B. Kibble, G. Lazarides, and Q. Shafi. Strings in $so(10)$. *Physics Letters B*, 113(3):237 – 239, 1982.
- [37] T.W. B. Kibble. *Topological Defects and the Non-Equilibrium Dynamics of Symmetry Breaking Phase Transitions*, volume 549. Springer Netherlands, 2000.
- [38] There are several ways to call phases of spin-1 BECs. In this Letter, we apply the way used in the phase diagram of the review paper [12] (see Fig. 3 and Table 5 therein) with an aim to clearly specify the influence of the Zeeman shift while the region of antiferromagnetic interaction in the phase diagram is sometimes called “the polar phase” regardless of the Zeeman shift. It is noted that the AF and P phases are also called the easy-plane-polar (EPP) and easy-axis-polar (EAP) phases, respectively. .
- [39] Seji Kang, Sang Won Seo, Hiromitsu Takeuchi, and Y. Shin. Observation of Wall-Vortex Composite Defects in a Spinor Bose-Einstein Condensate. *Phys. Rev. Lett.*, 122:095301, Mar 2019.
- [40] Seji Kang, Deokhwa Hong, Joon Hyun Kim, and Y. Shin. Crossover from weak to strong quench in a spinor Bose-Einstein condensate. *Phys. Rev. A*, 101:023613, Feb 2020.
- [41] Takafumi Kita. Unconventional vortices and phase transitions in rapidly rotating superfluid ^3He . *Phys. Rev. B*, 66:224515, Dec 2002.
- [42] M. A. Silaev, E. V. Thuneberg, and M. Fogelström. Lifshitz Transition in the Double-Core Vortex in $^3\text{He-B}$. *Phys. Rev. Lett.*, 115:235301, Dec 2015.
- [43] Kenichi Kasamatsu, Ryota Mizuno, Tetsuo Ohmi, and Mikio Nakahara. Effects of a magnetic field on vortex states in superfluid $^3\text{He-B}$. *Phys. Rev. B*, 99:104513, Mar 2019.
- [44] Masaki Tange and Ryusuke Ikeda. Half-quantum vortex pair in the polar-distorted B phase of superfluid ^3He in aerogels. *Phys. Rev. B*, 101:094512, Mar 2020.
- [45] Robert C. Regan, J. J. Wiman, and J. A. Sauls. Vortex phase diagram of rotating superfluid $^3\text{He-B}$. *Phys. Rev. B*, 101:024517, Jan 2020.
- [46] Subroto Mukerjee, Cenke Xu, and J. E. Moore. Topological Defects and the Superfluid Transition of the $s = 1$ Spinor Condensate in Two Dimensions. *Phys. Rev. Lett.*, 97:120406, Sep 2006.
- [47] A. J. A. James and A. Lamacraft. Phase Diagram of Two-Dimensional Polar Condensates in a Magnetic Field. *Phys. Rev. Lett.*, 106:140402, Apr 2011.
- [48] Michikazu Kobayashi. Berezinskii-Kosterlitz-Thouless Transition of Spin-1 Spinor Bose Gases in the Presence of the Quadratic Zeeman Effect. *Journal of the Physical Society of Japan*, 88(9):094001, 2019.
- [49] D. T. Son and M. A. Stephanov. Domain walls of relative phase in two-component Bose-Einstein condensates. *Phys. Rev. A*, 65:063621, Jun 2002.
- [50] Marek Tylutki, Lev P. Pitaevskii, Alessio Recati, and Sandro Stringari. Confinement and precession of vortex pairs in coherently coupled Bose-Einstein condensates. *Phys. Rev. A*, 93:043623, Apr 2016.
- [51] Minoru Eto and Muneto Nitta. Confinement of half-quantized vortices in coherently coupled Bose-Einstein condensates: Simulating quark confinement in a QCD-like theory. *Phys. Rev. A*, 97:023613, Feb 2018.
- [52] A. Gallemí, L. P. Pitaevskii, S. Stringari, and A. Recati. Decay of the relative phase domain wall into confined vortex pairs: The case of a coherently coupled bosonic mixture. *Phys. Rev. A*, 100:023607, Aug 2019.
- [53] Christopher J Pethick and Henrik Smith. *Bose-Einstein condensation in dilute gases*. Cambridge university press, 2008.
- [54] Tetsuo Ohmi and Kazushige Machida. Bose-Einstein condensation with internal degrees of freedom in alkali atom gases. *Journal of the Physical Society of Japan*, 67(6):1822–1825, 1998.
- [55] M. M. Salomaa and G. E. Volovik. Vortices with Ferromagnetic Superfluid Core in $^3\text{He-B}$. *Phys. Rev. Lett.*, 51:2040–2043, Nov 1983.
- [56] Shinsuke Hayashi, Makoto Tsubota, and Hiromitsu Takeuchi. Instability crossover of helical shear flow in segregated Bose-Einstein condensates. *Phys. Rev. A*, 87:063628, Jun 2013.
- [57] Haskell B Curry. The method of steepest descent for non-linear minimization problems. *Quarterly of Applied Mathematics*, 2(3):258–261, 1944.
- [58] See Supplemental Material for details of the numerical method and cross-section profiles for different values of q/μ . .
- [59] Neglecting the spin interaction with $\frac{c_1}{c_0} = 0.016 \ll 1$, the critical value is determined $q_C/\mu \approx 0.25$ by regarding $\Phi_{\pm 1}$ as a single-particle wave function bounded by the vortex core of Φ_0 . A similar problem is solved for the nematic-spin vortex in the AF phase [60]. .
- [60] Andrew P. C. Underwood, D. Baillie, P. Blair Blakie, and H. Takeuchi. Properties of a nematic spin vortex in an antiferromagnetic spin-1 Bose-Einstein condensate. *Phys. Rev. A*, 102:023326, Aug 2020.
- [61] I-Kang Liu, Shih-Chuan Gou, and Hiromitsu Takeuchi.

- Phase diagram of solitons in the polar phase of a spin-1 bose-einstein condensate. *Phys. Rev. Research*, 2:033506, Sep 2020.
- [62] A similar rule has been introduced in the absence of the quadratic Zeeman effect; Tomoya Isoshima, Kazushige Machida, and Tetsuo Ohmi, *Quantum Vortex in a Spinor Bose-Einstein Condensate*, J. Phys. Soc. Jpn. **70**, 1604 (2001) .
- [63] L. M. Milne-Thomson. *Theoretical aerodynamics*. (Dover Publications, New York, 2012).
- [64] See Supplemental Material for details of the derivation of the hydrodynamic potential. .
- [65] A similar behavior was also found in the continuous phase transition of the core state of soliton and vortex in spinor BECs [60, 61] .
- [66] See Supplemental Material for details of the computation of the spin interaction. .
- [67] E. M. Lifshitz and L. P. Pitaevskii. *Statistical physics*. Part 2 edited by L. D. Landau and E. M. Lifshitz (Pergamon Press, New York, 1980) Vol. 9.
- [68] In a rotating frame, the local superfluid velocity at the surface of the condensate is estimated as $\mathbf{v}_0 = (v_\varphi - R\Omega)\hat{\varphi}$ with $v_\varphi \sim \frac{\hbar}{MR_\perp}$. When the velocity exceeds a critical value, comparable to the phonon velocity $\sqrt{\mu/M}$, the vortex nucleation occurs after the excitation of ripples due to the Landau instability at the surface. .
- [69] G Volovik. Half-quantum vortices in superfluid $^3\text{He-B}$. *JETP Lett*, 52(6):358, 1990.
- [70] Minoru Eto, Kenichi Kasamatsu, Muneto Nitta, Hiromitsu Takeuchi, and Makoto Tsubota. Interaction of half-quantized vortices in two-component Bose-Einstein condensates. *Phys. Rev. A*, 83:063603, Jun 2011.
- [71] Justin Lovegrove, Magnus O. Borgh, and Janne Ruostekoski. Energetically stable singular vortex cores in an atomic spin-1 Bose-Einstein condensate. *Phys. Rev. A*, 86:013613, Jul 2012.
- [72] Although type-II HQVs have been numerically realized under rotation [73, 74], they did not distinguish physically type-I and type-II by neglecting the impact of the domain wall. .
- [73] Magnus O. Borgh, Muneto Nitta, and Janne Ruostekoski. Stable Core Symmetries and Confined Textures for a Vortex Line in a Spinor Bose-Einstein Condensate. *Phys. Rev. Lett.*, 116:085301, Feb 2016.
- [74] Justin Lovegrove, Magnus O. Borgh, and Janne Ruostekoski. Stability and internal structure of vortices in spin-1 Bose-Einstein condensates with conserved magnetization. *Phys. Rev. A*, 93:033633, Mar 2016.
- [75] Y. Kondo, J. S. Korhonen, M. Krusius, V. V. Dmitriev, E. V. Thuneberg, and G. E. Volovik. Combined spin-mass vortex with soliton tail in superfluid $^3\text{He-B}$. *Phys. Rev. Lett.*, 68:3331–3334, Jun 1992.
- [76] Olli V. Lounasmaa and Erkki Thuneberg. Vortices in rotating superfluid ^3He . *Proceedings of the National Academy of Sciences*, 96(14):7760–7767, 1999.
- [77] Kenichi Kasamatsu, Makoto Tsubota, and Masahito Ueda. Vortex Molecules in Coherently Coupled Two-Component Bose-Einstein Condensates. *Phys. Rev. Lett.*, 93:250406, Dec 2004.
- [78] Mattia Cipriani and Muneto Nitta. Crossover between Integer and Fractional Vortex Lattices in Coherently Coupled Two-Component Bose-Einstein Condensates. *Phys. Rev. Lett.*, 111:170401, Oct 2013.
- [79] Luca Calderaro, Alexander L. Fetter, Pietro Massignan, and Peter Wittek. Vortex dynamics in coherently coupled Bose-Einstein condensates. *Phys. Rev. A*, 95:023605, Feb 2017.
- [80] Kousuke Ihara and Kenichi Kasamatsu. Transverse instability and disintegration of a domain wall of a relative phase in coherently coupled two-component Bose-Einstein condensates. *Phys. Rev. A*, 100:013630, Jul 2019.
- [81] Michikazu Kobayashi, Minoru Eto, and Muneto Nitta. Berezinskii-Kosterlitz-Thouless Transition of Two-Component Bose Mixtures with Intercomponent Josephson Coupling. *Phys. Rev. Lett.*, 123:075303, Aug 2019.
- [82] Kohsuke Yagi, Tetsuo Hatsuda, and Yasuo Miake. *Quark-gluon plasma: From big bang to little bang*, volume 23. Cambridge University Press, 2005.

SUPPLEMENTAL MATERIAL

Method of the numerical simulation

Here, we describe the method of numerical simulation used in this work. The numerical solutions are obtained by minimizing the energy functional

$$G'' = \int_{-R_1}^{R_1} dx \int_{-R_2}^{R_2} dy \int_{-R_3}^{R_3} dz d^3x (\mathcal{G} + V_{\text{trap}}n - \Omega l_z)$$

with the trapping potential V_{trap} and $l_z = \hbar \sum_m \Re[\Phi_m x \partial_y \Phi_m - y \partial_x \Phi_m]$. The space coordinates $(x, y, z) = (x_1, x_2, x_3)$ are discretized as $x_i(n_i) = -R_i + \Delta x n_i$ with $n_i = 0, 1, 2, \dots, N_i$ with $x_i(N_i) = R_i$. The spatial derivatives of Φ_m are computed with finite difference approximation; e.g., $\partial_x \Phi_m$ and $\partial_x^2 \Phi_m$ are computed by the central difference of the first and second order, respectively.

All solutions were obtained by minimizing the energy functional very carefully. The steepest descent method is performed by solving the imaginary time evolution $\frac{\partial \Phi_m}{\partial \tau} = -\frac{\delta G''}{\delta \Phi_m}$. The imaginary time τ is discretized as $\tau = \Delta \tau n_\tau$ with $n_\tau = 0, 1, 2, \dots$. The time evolution is written as $\Phi_m(n_\tau + 1) = \Phi_m(n_\tau) - \Delta \tau \frac{\delta G''}{\delta \Phi_m}(n_\tau)$. The evolutions were computed until the difference $G''(n_\tau) - G''(n_\tau - 1000)$ becomes non-negative within the double precision by using Intel[®] Fortran Compiler.

The solutions in a uniform system is approximately obtained in a cylindrical box potential $V_{\text{trap}} = V_0 [\tanh(r - R) + 1]$ with $V_0/\mu = 20$, $R = 0.95R_\perp$, and $R_1 = R_2 = R_\perp$. Here, we solve two-dimensional equations by assuming that the wave functions are homogeneous along the z axis and thus independent of z . The trap depth V_0 is taken to be so large that the order parameter damps quickly outside the cylinder and almost vanishes nearby the system boundary. The boundary effect becomes significant only when the distance l_{spin} between the spin spots becomes $\gtrsim R_\perp/2$. The system size is set to be enough large to neglect the boundary effect for the results in the main

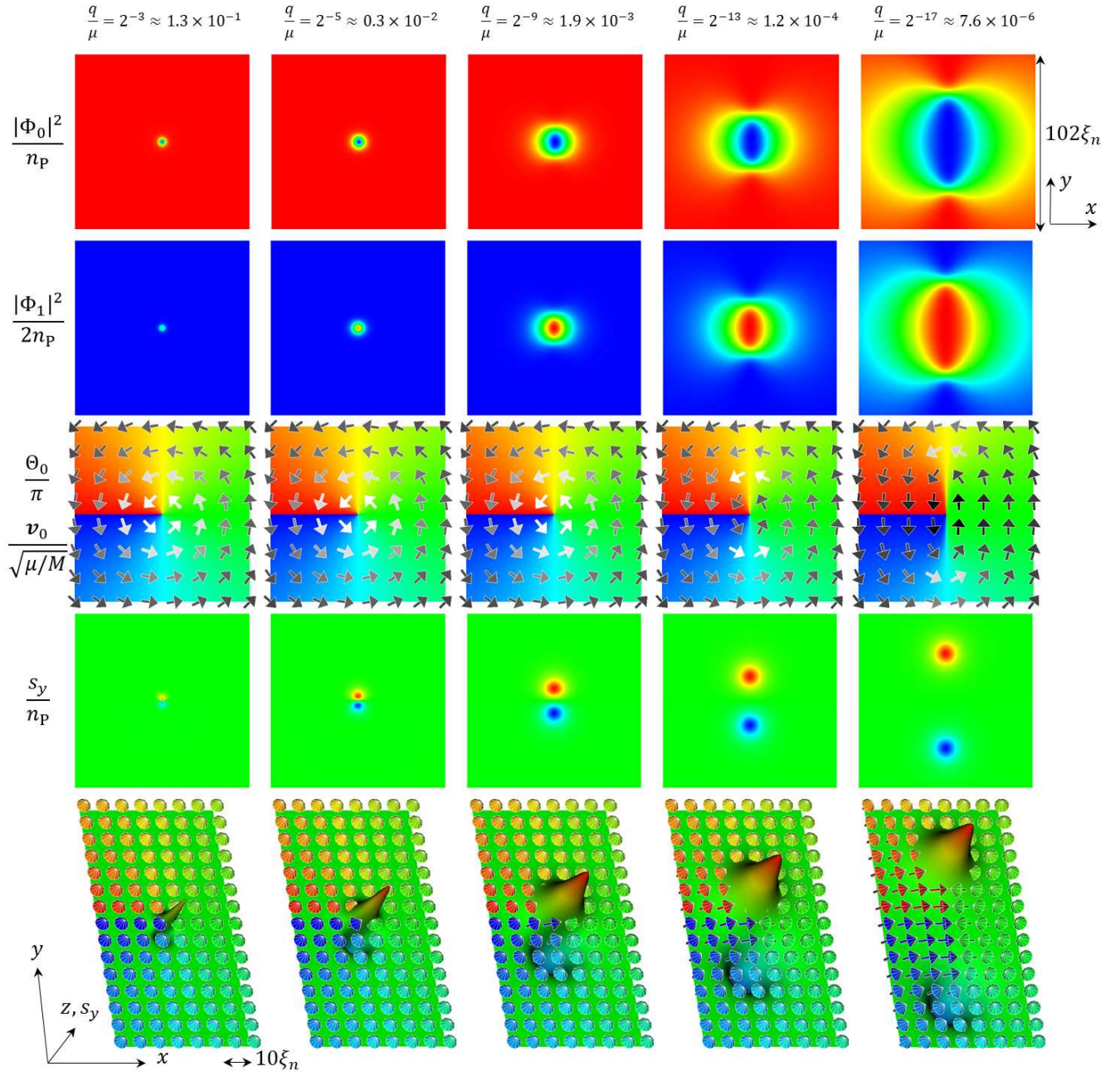


FIG. A1. The cross-sectional profiles of elliptic vortices and the three dimensional texture of pseudo-director field $\mathbf{g}/|\mathbf{g}|$ for $q = 2^{-n_q}$ ($n_q = 3, 5, 9, 13, 17$). The method of plot is the same as that of Fig. 1 in the main text. The angle of view is changed from that in Fig. 1 in the three dimensional plots in the bottom.

text. For the non-rotating case of $\Omega = 0$ (the results of Figs. 1 and 2), the numerical simulation was done with $2R_{\perp} = 1024.5\xi_n$ with $N_1 = N_2 = 2048$, $\Delta x = 0.5\xi_n$, and $\Delta\tau = 0.0025$. It was confirmed that our results do not change essentially for $\Delta x = 0.3\xi_n$ and $\Delta x = 0.4\xi_n$ except for the finite-size effect, which is of no interest to our main subject. The finite-size effect becomes important only for $\frac{q}{\mu} \leq 2^{-19} \approx 1.9 \times 10^{-6}$ for $\Delta = 0.5\xi_n$. For very small values of $\frac{q}{\mu}$ the width of the elliptic vortex become on the order of or larger than the system size and

we could not obtain the vortex state.

The vortex solutions were obtained for $q/\mu = 2^{-n_q}$ ($n_q = 0, 1, 2, \dots$) as shown in Fig. A1. The vortex has the normal core with $\Phi_{\pm 1} = 0$ for $n_q < 3$ (not shown). The protocol of the numerical simulation is as follows. First, the solution for $n_q = 3$ is obtained. Then, the initial state of the time evolution is set as $\Phi_0 = f_0(r)e^{i\varphi}$ and $\Phi_{\pm 1} = f_{\pm 1}$ with $f_0(r) = \sqrt{\max(0, n'_{\text{TF}})}$, $n'_{\text{TF}} = c_0^{-1}(\mu - V_{\text{trap}} - \frac{\hbar^2}{2Mr^2})$ and $f_{\pm 1}(r) = \pm \sqrt{\frac{n_{\text{P}}}{2}} e^{-r^2/\xi_n^2}$. The vortex can be stabilized in the center region even for the

non-rotating case of $\Omega = 0$ since the spatial gradient of V_{trap} is negligibly small there. The solution for $n_q + 1$ is obtained by using the solution of n_q as the initial state.

The rotating case of Fig. 3 (a) is obtained with $2R_{\perp} = 410\xi_n$ with $N_1 = N_2 = 1048$ and $\Delta = 0.4\xi_n$. The protocol is the same as the non-rotating case. For the three dimensional simulation in the harmonic trap of Fig. 3 (b), the system size is $2R_{\perp} = 192.5\xi_n$ and $2R_z = 128.5\xi_n$ with $N_1 = N_2 = 384$, $N_3 = 256$ and $\Delta = 0.5\xi_n$. In the local density approximation, the effective chemical potential is written as $\mu' = \mu - V_{\text{trap}}$. According to Fig. 2(b), the spin density decreases with q/μ' . This is why the spin poles becomes thinner as they are away from the trap center. The vortex core size becomes thicker as the local healing length $\frac{\hbar}{\sqrt{M\mu'}}$ becomes larger for large $|z|$.

Computation of the hydrodynamic potential

The velocity field $\mathbf{v} = (u, v)^T$ in a two dimensional potential flow is represented as $u = \partial_y \Psi = \partial_x \Phi$ and $v = -\partial_x \Psi = \partial_y \Phi$ with the Stream function Ψ and the velocity potential Φ . The complex velocity potential $W = \Phi + i\Psi$ of a point vortex with a circulation Γ in the complex plane (x, y) is written as $W = -i\frac{\Gamma}{2\pi} \log z$. The Joukowski transformation $z = \zeta + \frac{a^2}{\zeta}$ with $\zeta = ae^{\phi+i\psi}$ reads $x = 2a \cosh \phi \cos \psi$ and $y = 2a \sinh \phi \sin \psi$. This transformation corresponds to a mapping from a circle of radius a to an ellipse of major radius $2a \cosh \phi$ and minor radius $2a \sinh \phi$ ($\phi \geq 0$) in the xy plane. The ellipse reduces a segment of length $4a$ along the x axis for $\phi = 0$. The segment is along the y axis if a is replaced by ia in the formula of ζ . We used the formula $\zeta = ae^{\phi+i\psi}$ in the following computation without loss of generality.

In a quantized vortex in a scalar superfluid, the velocity field diverges at the center of the vortex core, where the order parameter amplitude vanishes at the core. The density increases to the bulk value far from the core. The region within a circle of a radius ξ_n with small density around the center is called the core region. To evaluate the energy of a quantized vortex per unit length, the contributions from the core region ($r < \xi_n$) and its outer region ($r > \xi_n$) is computed separately. Similarly, for the elliptic vortex, there exists the core region of an elliptic form around the band-shaped singularity and the energy is computed separately.

To compute the energy analytically, we neglect the so-called quantum pressure term in the Thomas-Fermi (TF) approximation [53]. Then, the density far from the vortex core can be written as

$$n \approx n_{\text{TF}} = n_{\text{bulk}} \left(1 - \frac{M}{2\mu} \mathbf{v}^2 \right)$$

with $n_{\text{bulk}} = n_{\text{P}}$ is the bulk density. In this approximation, one obtains the contribution to the energy functional G from the outer region of area S_{out} up to the

order of $\mathcal{O} \left(\frac{M}{2\mu} \mathbf{v}^2 \right)$,

$$\begin{aligned} E_{\text{out}} &= \int_{S_{\text{out}}} d^2x \mathcal{G} \\ &\approx \int_{S_{\text{out}}} d^2x \left[\frac{Mn_{\text{TF}}}{2} \mathbf{v}^2 + \mathcal{U}(n_{\text{TF}}) \right] \\ &= \int_{S_{\text{out}}} d^2x \left[\frac{Mn_{\text{P}}}{2} \mathbf{v}^2 + \mathcal{U}_{\text{P}} \right]. \end{aligned} \quad (\text{A1})$$

Here, $\mathcal{U}(n_{\text{TF}})$ is the energy density \mathcal{U} evaluated in the TF approximation, and it reduces to, for the bulk P phase,

$$\mathcal{U}_{\text{bulk}} = \mathcal{U}_{\text{P}} = -\frac{\mu^2}{2c_0}.$$

A local state, different from the P state, appears in the core region where the $m = 0$ component vanishes. The contribution from the core region is written as

$$E_{\text{core}} = \mathcal{U}_{\text{core}} S_{\text{core}}$$

with the energy density $\mathcal{U}_{\text{core}}$ and the area S_{core} of the core region.

The vortex energy E_{vortex} is defined as an excess energy in the presence of the vortex, the difference between the total energy with a vortex and the energy $E_{\text{bulk}} = \mathcal{U}_{\text{bulk}}(S_{\text{core}} + S_{\text{out}})$ in the absence of it;

$$\begin{aligned} E_{\text{vortex}} &= E_{\text{out}} + E_{\text{core}} - E_{\text{bulk}} \\ &= U_{\text{out}} + U_{\text{core}} \end{aligned} \quad (\text{A2})$$

with $U_{\text{core(out)}} = E_{\text{core(out)}} - \mathcal{U}_{\text{P}} S_{\text{core(out)}}$. The potentials of the outer and core regions are rewritten as

$$\begin{aligned} U_{\text{out}} &= \frac{Mn_{\text{bulk}}}{2} \int_{S_{\text{out}}} d^2x \mathbf{v}^2 \\ U_{\text{core}} &= \delta \mu n_{\text{bulk}} S_{\text{core}} \end{aligned} \quad (\text{A3})$$

with $\delta = \frac{\mathcal{U}_{\text{core}}}{\mu n_{\text{bulk}}} + \frac{1}{2}$.

The potential U_{out} , which is reduced to the hydrodynamic potential U_{hyd} as shown later, is evaluated by computing the integral

$$\begin{aligned} I &= \int_{S_{\text{out}}} dx dy \mathbf{v}^2 \\ &= \left(\frac{\Gamma}{2\pi} \right)^2 \int_{S_{\text{out}}} dx dy \left| \frac{1}{\sqrt{z^2 - 4a^2}} \right|^2 \\ &= \left(\frac{\Gamma}{2\pi} \right)^2 \int_{S_{\text{out}}} dx dy \frac{1}{\sqrt{(x^2 - y^2 - 4a^2)^2 + 4x^2 y^2}}. \end{aligned}$$

Here, we used

$$|u| = \frac{\Gamma}{2\pi} \left| \Im \left[\frac{\partial_x \zeta}{\zeta} \right] \right| = \frac{\Gamma}{2\pi} \left| \Im \left[\frac{1}{\sqrt{z^2 - 4a^2}} \right] \right|$$

and

$$|v| = \frac{\Gamma}{2\pi} \left| \Im \left[\frac{\partial_y \zeta}{\zeta} \right] \right| = \pm \frac{\Gamma}{2\pi} \left| \Re \left[\frac{1}{\sqrt{z^2 - 4a^2}} \right] \right|.$$

According to the transformation (for the ellipse along the x axis)

$$(x, y) = (2a \cosh \phi \cos \psi, 2a \sinh \phi \sin \psi)$$

we have the determinant of the Jacobian matrix

$$\left| \frac{\partial(x, y)}{\partial(\phi, \psi)} \right| = 2a^2 (\cosh 2\phi - \cos 2\psi).$$

The integral I is computed as

$$\begin{aligned} I &= \left(\frac{\Gamma}{2\pi} \right)^2 \int_{\phi_{\text{core}}}^{\phi_R} d\phi \int_{-\pi}^{\pi} d\psi \frac{1}{2a^2 \sqrt{(\cosh 2\phi - \cos 2\psi)^2}} \left| \frac{\partial(x, y)}{\partial(\phi, \psi)} \right| \\ &= \frac{\Gamma^2}{2\pi} \int_{\phi_{\text{core}}}^{\phi_R} d\phi \\ &= \frac{\Gamma^2}{2\pi} (\phi_R - \phi_{\text{core}}) \\ &= \frac{\Gamma^2}{2\pi} \ln \frac{\rho_R}{\rho_{\text{core}}} \end{aligned}$$

with the radius of the system boundary in the ζ plane

$$\rho_R = ae^{\phi_R} \text{ or } \phi_R = \ln \frac{\rho_R}{a}$$

and the cutoff radius for the core region

$$\rho_{\text{core}} = ae^{\phi_{\text{core}}} \text{ or } \phi_{\text{core}} = \ln \frac{\rho_{\text{core}}}{a} \quad (\rho_{\text{core}} > a).$$

The system boundary and the cutoff circle in the ζ plane are mapped into ellipses in the xy plane. The major and minor radiuses are written as

$$\begin{aligned} A_{R,\text{core}} &= 2a \cosh \phi_{R,\text{core}} = \frac{\rho_{R,\text{core}}^2 + a^2}{\rho_{R,\text{core}}} \\ B_{R,\text{core}} &= 2a \sinh \phi_{R,\text{core}} = \frac{\rho_{R,\text{core}}^2 - a^2}{\rho_{R,\text{core}}} \end{aligned} \quad (\text{A4})$$

and they satisfy the relation

$$A_{R,\text{core}} + B_{R,\text{core}} = 2\rho_{R,\text{core}}.$$

Here, A_{core} and B_{core} correspond to R_+ and R_- in the main text, respectively. In the limit $\frac{\rho_R}{a} \rightarrow \infty$, we have

$$A_R = B_R \rightarrow \rho_R = R$$

with the radius R of the system boundary in the xy plane.

The size of the core region is parametrized by two parameters, a and

$$r_{\text{core}} \equiv \rho_{\text{core}} - a.$$

Then, we have

$$U_{\text{out}} \approx U_{\text{hyd}} = \frac{Mn_{\text{P}}}{2} \frac{\Gamma^2}{2\pi} \ln \frac{R}{a + r_{\text{core}}}.$$

The area S_{core} of the core region is represented as

$$S_{\text{core}} = \pi A_{\text{core}} B_{\text{core}} = \pi \frac{(a + r_{\text{core}})^4 - a^4}{(a + r_{\text{core}})^2}$$

The oblateness f of the core region is defined as

$$f = 1 - \frac{B_{\text{core}}}{A_{\text{core}}} = \frac{2}{1 + (1 + r_{\text{core}}/a)^2}.$$

For $\frac{r_{\text{core}}}{a} \ll 1$, asymptotic to the limit of the maximum oblateness ($f = 1$), we have

$$A_{\text{core}} \approx 2a, \quad B_{\text{core}} \approx 2r_{\text{core}}$$

and for $\frac{r_{\text{core}}}{a} \gg 1$, asymptotic to the limit of the minimum oblateness ($f = 0$),

$$A_{\text{core}} = B_{\text{core}} \approx r_{\text{core}}.$$

The former limit corresponds to a vortex with a band-shaped core region in three dimensions, called a vortex band. The latter corresponds to a conventional vortex filament with cylindrical core region.

Computation of the spin interaction

The local BA state, emerging around the edge of the elliptic vortex, is collateral in the existence of the local AF state in the vortex center. Therefore, the magnetization can be associated with the density at the origin $n_{\text{core}} = n(\mathbf{r} = 0)$. According to the mean-field approach in the previous studies [60, 61], a continuous phase transition occurs at a critical point ($q = q_C$) in the core of a topological defect. This approach is also well applicable to our case. We obtain similar behaviors $n_{\text{core}} \propto 1 - \frac{q}{q_C}$ and $s_y^{\text{max}} = \max s_y \propto \sqrt{1 - \frac{q}{q_C}}$. Since the density is asymptotic to n_{AF} far from the critical point for $q \ll q_C$, a quantitative estimation is obtained by

$$n_{\text{core}} \sim n_{\text{AF}} \left(1 - \frac{q}{q_C} \right),$$

which is quantitatively agreed with the numerical result [Fig. 2(b)].

The magnetization is well described with this approach too. The magnetization happens in the two spin spots with $\arg \Phi_0 = \pm\pi$ along the y axis. Then the local spin density is written as $F_y \sim \pm 2\sqrt{2n_1} |\Phi_0|^2$ with $\Phi_{+1} = -\Phi_{-1} = \sqrt{n_1} \propto \sqrt{n_{\text{core}}}$. The density is almost constant $n \approx n_{\text{P}}$ everywhere for small q and then the maximum value is estimated by the relation between the arithmetic and geometric means with $2n_1 = \frac{n}{2} \approx \frac{n_{\text{core}}}{2}$ and $|\Phi_0|^2 = \frac{n}{2} \approx \frac{n_{\text{P}}}{2}$ as

$$s_y^{\text{max}} \sim \frac{\sqrt{n_{\text{core}} n_{\text{P}}}}{1 + \frac{c_2}{c_0}},$$

where the factor in the denominator comes from the spin interaction in the presence of spin density.

The size r_{spin} of the magnetic spot around the edges grows with the size of the AF-core, $\sim \xi_q$. The spin interaction becomes more important as the magnetic spot grows and the spot size finally reaches the spin healing length, estimated as

$$\xi_s = \frac{\hbar}{\sqrt{M\sigma}}$$

with $\sigma = c_2 n_{\text{P}}$. This crossover behavior of the spot size is described by a simple formula

$$r_{\text{spin}} = \frac{1}{\xi_s^{-1} + C_{\text{spin}} \xi_q^{-1}},$$

with a constant $C_{\text{spin}} \sim \mathcal{O}(1)$. Finally, the spin interaction energy is evaluated as

$$E_{\text{spin}} \sim \frac{1}{2} c_2 (s_y^{\text{max}})^2 \pi r_{\text{spin}}^2 \sim \frac{\pi}{2} \frac{c_2}{c_0} \frac{n_{\text{core}}}{n_{\text{P}}} \left(\frac{r_{\text{spin}}}{\xi_n} \right)^2 \mu n_{\text{P}} \xi_n^2.$$

This formula is well-consistent with the numerical result with $C_{\text{spin}} = 0.8$.